Molecular Therapy
Methods & Clinical Development
Original Article

Kinetics and MR-Based Monitoring of AAV9 Vector Delivery into Cerebrospinal Fluid of Nonhuman Primates

Kousaku Ohno,[1,4] Lluis Samaranch,[1,4] Piotr Hadaczek,[1] John R. Bringas,[1] Philip C. Allen,[2] Vivek Sudhakar,[1] Diane E. Stockinger,[2] Christopher Snieckus,[1] Michael V. Campagna,[2] Waldy San Sebastian,[1] Jerusha Naidoo,[1] Haifeng Chen,[3] John Forsayeth,[1] Ernesto A. Salegio,[2] Granger G.C. Hwa,[2] and Krystof S. Bankiewicz[1]

[1]Department of Neurological Surgery, University of California, San Francisco, San Francisco, CA 94103, USA; [2]Valley Biosystems, Inc., West Sacramento, CA 95605, USA; [3]Virovek, Inc., Hayward, CA 94541, USA

Here we evaluated the utility of MRI to monitor intrathecal infusions in nonhuman primates. Adeno-associated virus (AAV) spiked with gadoteridol, a gadolinium-based MRI contrast agent, enabled real-time visualization of infusions delivered either via cerebromedullary cistern, lumbar, cerebromedullary and lumbar, or intracerebroventricular infusion. The kinetics of vector clearance from the cerebrospinal fluid (CSF) were analyzed. Our results highlight the value of MRI in optimizing the delivery of infusate into CSF. In particular, MRI revealed differential patterns of infusate distribution depending on the route of delivery. Gadoteridol coverage analysis showed that cerebellomedullary cistern delivery was a reliable and effective route of injection, achieving broad infusate distribution in the brain and spinal cord, and was even greater when combined with lumbar injection. In contrast, intracerebroventricular injection resulted in strong cortical coverage but little spinal distribution. Lumbar injection alone led to the distribution of MRI contrast agent mainly in the spinal cord with little cortical coverage, but this delivery route was unreliable. Similarly, vector clearance analysis showed differences between different routes of delivery. Overall, our data support the value of monitoring CSF injections to dissect different patterns of gadoteridol distribution based on the route of intrathecal administration.

INTRODUCTION

We have previously demonstrated the value of monitoring parenchymal brain infusions of adeno-associated virus (AAV) and the correlation between post-mortem biodistribution of the viral vector and gadolinium contrast on MRI.[1–3] Over the years, by means of magnetic resonance (MR)-guided intraparenchymal convection-enhanced delivery (CED), we have achieved transduction of large areas of the cortex by infusing viral vector into specific subcortical structures. For example, thalamic infusion of AAV directs efficient widespread expression of the transgene in the cortex through thalamo-cortical pathways.[4] Also, MR-guided CED infusions of AAV2 vector into nonhuman primate (NHP) putamen and substantia nigra supported current first-in-human clinical trials in Parkinson's disease (ClinicalTrials.gov: NCT01973543 and NCT01621581) and Aromatic L-amino Acid Decarboxylase (AADC) deficiency (ClinicalTrials.gov: NCT02852213). These direct brain infusions have remarkable clinical value in diseases with a compartmented pathological component. However, in pathologies where broad transduction is desirable, dissemination of the viral particles via cerebrospinal fluid (CSF) may be preferable to achieve complete nervous system transduction.

CSF is continuously produced by the choroid plexus epithelium within the lateral, third, and fourth brain ventricles,[5,6] and it flows through the CNS before reaching the major sites of reabsorption located in the arachnoid villi and the primitive lymphatic system at the cribriform plate.[7] This fluid dynamic makes vector distribution via intrathecal delivery challenging.[8–16] CSF delivery through subarachnoid space puncture at the lumbar level is the standard operative intrathecal delivery. Computed tomography (CT)-fluoroscopic guidance or ultrasonography (US) guidance is required to confirm the correct location of the needle and to avoid medullary injuries that can cause sensory and motor complications.[17] Although CT-fluoroscopic guidance or US guidance has decreased the incidence of traumatic lumbar punctures compared to the non-guided landmark-based technique,[18,19] there are still several disadvantages that make these techniques sub-optimal to monitor the delivery of the infusate, such as limited soft-tissue visualization, image artifacts, and radiation exposure.

On the other hand, MRI enables a superior contrast resolution relative to CT and US, as well as high spatial resolution without the use of ionizing radiation.[20] In addition, the short duration of current high-resolution image acquisition protocols in the standard MR

Received 29 June 2018; accepted 3 December 2018;
https://doi.org/10.1016/j.omtm.2018.12.001.

[4]These authors contributed equally to this work.

Correspondence: Krystof S. Bankiewicz, Department of Neurological Surgery, University of California San Francisco, 1855 Folsom Street, MCB 226, San Francisco, CA 94103-0555, USA.
E-mail: krystof.bankiewicz@ucsf.edu

instruments enables the acquisition of real-time information before, during, and after administration of the therapeutic agent. There are three possible access sites for intrathecal delivery of AAV: lateral ventricle; lumbar; and cerebellomedullary cistern, also known as cisterna magna (CM). To the best of our knowledge, MR monitoring of these infusion techniques has not been performed. Here we analyzed the impact of these delivery routes on the reproducibility of delivery by monitoring each one of them with near real-time MRI during vector administration. To visualize the infusions, we co-infused the viral vector with gadoteridol (ProHance, Bracco Diagnostics, Princeton, NJ, USA), a gadolinium-based MRI contrast agent.

Real-time MRI is a useful tool for confirming the acute dynamics of infusate administered into the CSF. Given that the half-life of the contrast agent is short, there is, consequently, no guarantee that the contrast agent diffusion accurately reflects the vector diffusion. Examination of the kinetics of AAV9 vector in CSF at longer time points following CSF delivery would provide useful information on the distribution and potential excretion mechanism of the vector in CSF, and it would provide some insight into the delivery parameters required for successful CSF administration when combined with real-time MRI. In the present study, CSF was collected at several time points after AAV9 administration, and CSF vector concentration was measured. To our knowledge, this is the first description of the kinetics of CSF vector concentration after the administration of AAV9 vector into the CSF of NHPs. In this paper, we show that the combination of real-time MRI and measurement of CSF vector concentration detected a leakage of infusate and a subsequent decrease in the CSF vector concentration. Furthermore, kinetics parameters differed with respect to the route of CSF administration, suggesting that the elimination rate of AAV9 from CSF is affected by the injection site.

RESULTS

Real-Time MRI

All animals received 6 mL AAV9 carrying a human acid sphingomyelinase (ASM) with a C-terminal human influenza hemagglutinin (HA) tag (AAV9-hASM-HA) at a concentration of 2.2×10^{13} (vector genomes [vg]/mL), spiked with gadolinium chelate (2 mM, ProHance, Bracco Diagnostics, Princeton, NJ, USA) to monitor the delivery and distribution of the infusate. Five approaches were tested that combined different routes of administration: (1) acute administration (1 mL/min) by CM injection, (2) continuous administration (1 mL/hr) by CM injection, (3) acute administration (1 mL/min) by lumbar injection, (4) acute administration (1 mL/min) by combined CM and lumbar injection, and (5) acute administration (1 mL/min) by intracerebroventricular (i.c.v.) injection to lateral ventricle bilaterally. All the groups are summarized in Table S1. CSF delivery of AAV vectors by infusion into the CM, lumbar, and lateral ventricles did not lead to any adverse events in any of the treated animals.

Real-time MRI of the CM acute injection (n = 3) showed infusate distribution in the brain and spinal cord over time (Figure 1A). The gadoteridol signal was first detected in the CM, and it expanded throughout the CSF space at the base of the brain. Flow and distribution were consistent among all animals for the entire monitoring period. Distribution and volume analysis at the end of the infusion showed a consistent pattern of distribution in all the animals (Figure S1A). No MR tracer signal was visible in the images acquired after the CM continuous injection over 6 hr (n = 3). The low infusion rate (1 mL/hr) presumably allowed considerable dilution of tracer in the CSF below the limit of detection.

Real-time imaging of the lumbar acute injection (n = 3) detected individual variations of gadoteridol signal (Figure S1B). Although very similar progressive distribution from the infusion site was detected, the spread beyond spinal cord differed between animals. Further analysis revealed that two of the three animals that received lumbar injections had a strong tracer signal in the lumbar musculature surrounding the injection site. This hyper-intense signal suggests leakage of infusate, consistent with multiple dura tapping due to several attempts to place the needle, and it highlights the importance of dura preservation during lumbar injection to achieve brain and spinal cord distribution. Analysis of imaging from the animal in which the infusion was performed after a single puncture revealed complete gadoteridol coverage in the spinal cord and a limited frontal-ventral distribution of the tracer in the brain (Figure 1B).

Real-time MRI of the combined CM + lumbar acute injection (n = 2) showed a synergistic distribution in all the animals tested at the end of the monitoring. Combined delivery of the vector also revealed a time-dependent infusate distribution, with complete coverage of the spinal cord and almost complete cortical distribution (Figure 1C). Analysis of the volume distribution demonstrated that the combined delivery (3 mL CM and 3 mL lumbar) extended coverage beyond that seen in the CM (6 mL) and lumbar (6 mL) groups alone, resulting in increased cortical and spinal distribution of gadoteridol (Figure S1C).

Real-time MRI of the i.c.v. injection (n = 2) also showed a time-dependent infusate distribution in the brain and spinal cord (Figure 1D). In this case, analysis of the volume distribution consistently indicated much larger cortical distribution at the end of the acquisitions, including occipital cortical regions that were not covered by any other routes of delivery (Figure S1D). These data suggest that the i.c.v. delivery route directs almost complete distribution to the cortical and cerebellar regions.

Kinetic Analysis of Vector Infusate

To evaluate capsid clearance, CSF samples (~1 mL) were collected from the CM at 15 min, 30 min, 1 hr, 6 hr, 12 hr, 24 hr, and 28 days after AAV9 injection in all groups. Vector genome copies per milliliter CSF were measured by qPCR. Vector genomes were detectable in the CSF at all time points. Animals that underwent multiple dura punctures in the lumbar injection group were excluded from the qPCR analysis, because vector leakage into the musculature surrounding the injection site yielded incomplete vector delivery into the CSF, as shown in real-time MRI (Figure S1B, animals 8 and 9).

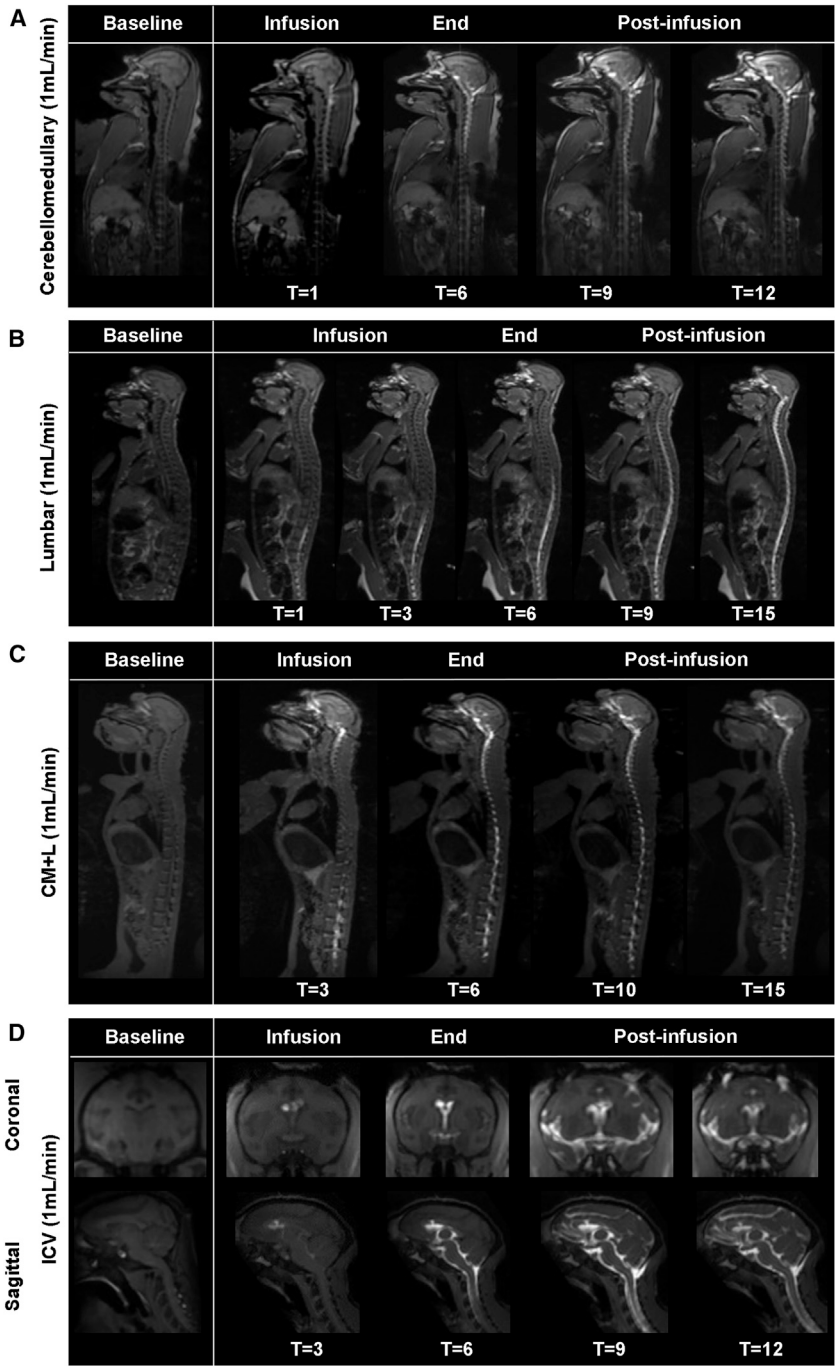

Figure 1. Monitoring of Gadolinium-Based MR Tracer Distribution by T1-Weighted Sequential MRI

Sagittal view of an MRI serial acquisition showing the tracer distribution in the CSF over time, up to 12–15 min after (A) acute CM injection, (B) lumbar injection, (C) combined CM + L injection, and (D) i.c.v. injection, of 6 mL viral vector spiked with 2 mM gadolinium at 1 mL/min. Abbreviations are as follows: MR, magnetic resonance; CM, cisterna magna (cerebellomedullary cistern); ICV, intracerebroventricular; L, lumbar; and T, time (min).

Five parameters were determined from the resulting qPCR data: maximum CSF concentration of vector (C_{max}), time of C_{max} (T_{max}), area under the titer-time curve from time 0 to 24 hr after the end of infusion (AUC_{24h}), AUC from time 0 to 28 days after the end of infusion (AUC_{28d}), and AUC extrapolated to infinity (AUC_{inf}) (see the Materials and Methods). Animals showed the C_{max} 15 min after the injection (T_{max}), regardless of the route of delivery with the sole exception of group 3, dosed in the lumbar region (Table S2). A case-by-case analysis revealed that the actual C_{max} value at CM differed between routes of delivery (Figures 2A–2D; Table S3), with CM acute delivery displaying the highest average vector concentration at T_{max}, followed by CM continuous, i.c.v., and CM + lumbar combination deliveries. After receiving half of the dose (3 mL) into the CM, the CM + lumbar combination showed approximately half of the C_{max} observed with the acute CM delivery ($3.0 \pm 0.5 \times 10^{12}$ vg/mL and $5.4 \pm 0.9 \times 10^{12}$ vg/mL, respectively). There was a time-dependent decrease in vector concentration over the 28 days after injection in all groups (Tables S2 and S3).

CSF vector concentration decreased rapidly in the i.c.v. infusion group compared to the other delivery routes (terminal half-life [$T_{1/2}$]: 2.3 ± 0.4 hr). Conversely, vector concentration decreased slowly in the CM + lumbar combined infusion group ($T_{1/2}$: 5.5 ± 2.1 hr). The $T_{1/2}$ values were comparable between the CM treatment groups (3.8 ± 0.8 hr and 4.1 ± 0.5 hr for the CM acute injection and the CM continuous injection groups, respectively) and intermediate compared to the i.c.v. and CM + lumbar combined infusion groups.

The AUC_{24h} value was lower with CM continuous infusion than with CM acute infusion ($7.8 \pm 3.2 \times 10^{12}$ hr × vg/mL compared to $22.9 \pm 8.6 \times 10^{12}$ hr × vg/mL). A similar trend was observed with the AUC_{28d} values ($29.5 \pm 15.4 \times 10^{12}$ hr × vg/mL and $111.5 \pm 75.6 \times 10^{12}$ hr × vg/mL in CM continuous infusion and CM acute infusion, respectively). For the CM + lumbar combined infusion, the AUC_{24h} and AUC_{28d} values were $17.1 \pm 1.8 \times 10^{12}$ hr × vg/mL and $109.8 \pm 51.2 \times 10^{12}$ hr × vg/mL, respectively. The $T_{1/2}$ of CM + lumbar combined infusion increased the AUC_{28d} at a similar rate to that of the acute CM infusion. The AUC_{24h} value in i.c.v. infusions was $10.5 \pm 5.7 \times 10^{12}$ hr × vg/mL.

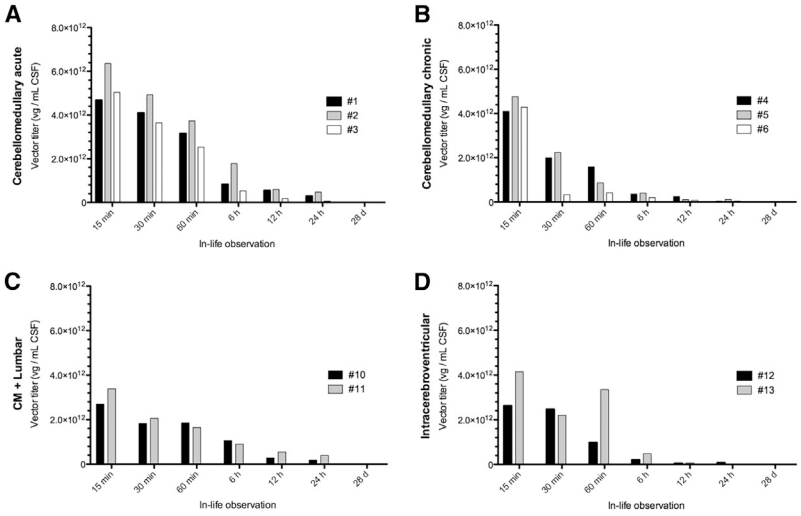

Figure 2. Vector Clearance for the Different Delivery Routes
CSF samples were collected at the CM level at multiple time points after the end of infusion. Vector load was evaluated by qPCR. Analysis of individual animal values showed a maximum concentration at 15 min after injection (T_{max}) in all the animals, irrespective of them having received the vector by acute CM (A), continuous CM (B), combined CM + L (C), or i.c.v. (D) route. Abbreviations are as follows: CSF, cerebrospinal fluid; CM, CM (cerebellomedullary cistern); ICV, intracerebroventricular; and L, lumbar.

DISCUSSION

In the present study, we investigated the utility of MRI in CSF delivery of AAV vectors in NHP, and we found that delivery route impacted both the distribution pattern of the infusate and the kinetics of AAV vector clearance. Real-time MRI and gadoteridol coverage analysis showed that CM delivery was an effective route of injection, achieving broad infusate distribution to the brain and spinal cord, and even greater distribution was observed when this was combined with lumbar injection. In contrast, i.c.v. injection resulted in strong cortical coverage but little spinal distribution. Lumbar injection alone led to the gadoteridol distribution primarily in the spinal cord, with little cortical coverage. Similarly, the vector genome analysis showed differences among groups, suggesting differential vector kinetics in the CSF based on the route of delivery.

Consecutive MR image acquisition showed that, after CM acute infusion at 1 mL/min, infusate flow resulted in almost complete gadoteridol coverage of the brain and spinal cord. Analysis of the gadoteridol signal over time revealed that, after filling the CM, the infusate descended dorsally along the spinal cord and then ascended ventrally to the brain before reaching the pre-frontal, frontal, and parietal areas of the brain. This sequence of infusate flow resulted in broader coverage of the spine than in the brain. The consequent lack of signal in occipital areas of the brain could be due to rapid drainage through the arachnoid granulations to the superior sagittal sinus. We also found that the AUC values in CM acute infusion were higher than those in CM continuous infusion. This difference would reflect the large interval from the beginning of administration to the first CSF collection in the CM continuous infusion group.

Acute lumbar injection resulted in primarily spinal cord distribution, a finding that is consistent with the natural flow of CSF in the spine that descends along the dorsal region of the spine and spinal canal and ascends through the ventral side to the base of the brain.[21] The absence of brain coverage with the lumbar injection could be due to insufficient infusate volume reaching the brain and/or intense dilution of gadoteridol in the CSF. Experiments with different volumes and infusion rates will enable precise predictions of infusate behavior after lumbar injection into the CSF. Lateral ventricle injections are widely used in clinical and preclinical studies to introduce a variety of drugs, plasmids, and viral vectors and circumvent the blood-brain barrier.[22–26] Our finding of more robust distribution of infusate in the brain than in the spinal cord was consistent with the natural flow of CSF from the lateral ventricle.

The analysis of the distribution of the gadoteridol signal in the i.c.v. injection group indicated that, after the infusate entered the lateral ventricles, the tracer was rapidly distributed throughout the ventricular system, filling up the third ventricle, descending to the fourth ventricle by the cerebral aqueduct, and reaching the spinal cord most likely through the lateral aperture.

A key finding from this study was the importance of real-time MRI to accomplish a complete and successful CSF delivery. This real-time monitorization allowed us to monitor the infusion, detect off-target signal like muscular leakage, and identify other aberrations causing lack of coverage. In addition, although further investigation is needed, another important feature of the real-time MR monitoring into the CSF is the potential to properly estimate the time course for intermittent or sequential delivery into the CSF in cases where the desired distribution is not obtained with a single infusion. Repeated injections into the CSF of low volumes in a very short time after visual confirmation could avoid high-pressure-based backflow through the cannula tract, achieving better fluid dynamics that could improve the flow and distribution of the infusate.[27] It is possible that intermittent i.c.v. dosing with smaller volumes could reduce the levels of unbound circulating AAV particles capable of triggering humoral immune responses. However, further experiments are required to test this hypothesis fully.

To evaluate the correlation among the spread of contrast reagent, the distribution pattern of AAV9-hASM-HA, and transgene expression, the brain and spinal cord were analyzed by immunostaining against the HA tag 28 days after CSF injection. Interestingly, in this study, HA-positive cells were found not only in the region in which the

gadoteridol signal was visible on MRI but also in parenchymal regions lacking gadoteridol signal (Figure S3). HA-positive cells were also present in the ventral horn of the cervical and lumbar sections (Figure S4). We have previously demonstrated a close correlation between Gd distribution and transgene expression after intraparenchymal AAV infusion.[1,28] These findings indicate that, with CSF delivery, the vector continues to diffuse beyond the gadoteridol signal, thereby transducing wider regions in contact with the CSF. We previously reported that CSF administration of AAV9-AADC[13] leads to robust cortical expression. However, transgene staining in the present study was weaker likely due to the low titer of the AAV used.

Our $T_{1/2}$ analysis suggested that delivery route affects clearance of AAV from the CSF. The similar $T_{1/2}$ values between the CM acute injection and CM continuous injection lead us to believe that AAV9 administered to CM follows the same excretion pathway regardless of the infusion rate. To the best of our knowledge, the excretion process of AAV from CSF has not been studied. A number of possible mechanisms could explain AAV disposition from the CSF. First, it is possible that this resulted from passive diffusion back across the blood-brain barrier and/or blood-CSF barrier. Although the CSF vector concentration was higher than the concentration in peripheral blood, passive diffusion from CSF to systemic blood would be unlikely because it would oppose the direction of CSF flow. Second, transporter-mediated delivery is also possible. However, although AAV receptors have been identified,[29] transporters for AAV have not been described thus far. We believe that biotransformation from the parent AAV configuration is also unlikely, because AAV capsid has been shown to be physiochemically stable in the extracellular matrix over prolonged periods of time.[30]

Cellular trafficking and uptake, on the other hand, are a likely contributing factor to the AAV clearance process from CSF. AAV vector is taken into the cell and exerts its effect by releasing its DNA into the nucleus.[31] It is well established that this process occurs via receptor-mediated endocytosis.[29] Further studies will enable us to discern the contribution of AAV cellular uptake to the clearance of AAV from CSF. Convection is also a plausible process by which AAV in CSF could be removed. CSF is produced by choroid plexus of the lateral ventricles.[5,32,33] The CSF in the lateral ventricles flows to the CM. It then bypasses the subarachnoid space in the spinal cord and is excreted to systemic blood.[5] Since CSF is not contained within a homogeneous compartment, it is possible that the sampling site affected the vector concentration. It would be useful in the future to measure and compare vector concentrations at several sampling sites. Furthermore, measurement of AAV titer in the blood would be useful to estimate biodistribution.

Unexpectedly, AUC_{inf} values calculated over 24 hr were approximately 6-fold lower than AUC_{28d} in the present study (Table S3), suggesting that AAV capsids persist in CSF for longer than expected. A possible explanation for this is reabsorption of AAV from the systemic blood into the CSF. When administered intravenously, AAV9 highly transduces neurons in the brain,[34] indicating that transfer of AAV between blood and CSF is possible. Thus, it is possible that, in the present study, AAV9 delivered into the CSF circulation was excreted into the peripheral blood and reabsorbed to the CNS, contributing to the long-term presence of AAV9 in CSF. Another possible mechanism is exocytosis of previously absorbed AAV from cells back into CSF. We have found that certain AAV serotypes are capable of undergoing *trans*-synaptic transport after injection into brain parenchyma,[35,36] and that the area of transgene expression with AAV2 infused to the NHP striatum increased over a period of 3 years when compared to 8 weeks after administration.[37] The AUC_{inf} values were calculated from data obtained in the first 24 hr after the end of infusion. The discrepancy between AUC_{inf} and AUC_{28d} suggests the possibility that the AUC_{inf} value would be different at longer time points after AAV administration. Further studies may enable us to determine whether this is the case.

Overall, the results of this first-in-primate exploratory study indicate that monitoring the infusion of AAV vectors coinfused with gadoteridol is a reliable method to assess the distribution of the infusate and any adverse events associated with delivery (like off target or backflow). The kinetics of AAV9 delivery into the CSF of NHP outlined here have the potential to significantly enhance the quality of the CSF delivery, which may inform clinical practices and have obvious implications for a number of neurological disorders.

MATERIALS AND METHODS

Animals

Adult Rhesus and Cynomolgus macaques (n = 13, 2.7–10.1 kg) were used in this study (Table S1). Animals were randomly assigned to CM acute infusion group (n = 3), CM continuous infusion group (n = 3), lumbar injection group (n = 3), CM + lumbar combination injection group (n = 2), and bilateral i.c.v. injection group (n = 2). Each animal received a single injection (6 mL) of a viral vector drive by a cytomegalovirus promoter and hosting a self-complementary DNA sequence of human ASM with a C-terminal HA tag (AAV9-hASM-HA) manufactured by Virovek (Hayward, CA, USA). On the day of surgery, a stock solution of the vector (2.20×10^{13} vg/mL) was spiked with 2 mM gadoteridol solution (ProHance, Bracco Diagnostics, Princeton, NJ, USA) and injected into the CSF.

All animals were tested for the presence of anti-AAV-neutralizing antibodies and considered seronegative (antibody titers <1:100).[38]

Qualified veterinary personnel monitored all animals daily throughout the study. All procedures were carried out in accordance with the Institutional Animal Care and Use Committee at Valley Biosystems (West Sacramento, CA).

Vector Delivery

CM Injection

Six animals were infused with vector into the CM. Briefly, after securing the head of the animal into an MR-compatible stereotactic frame, the head, neck, and back were shaved and prepared for the vector injection into the CSF. The animal was placed on inhaled

isoflurane (1%–3%) anesthesia, transferred to the MR suite, and was placed in sphinx position in the MR scanner bed. A pelvic phased-array surface coil was positioned over the head and upper neck region. Aseptic techniques were used to guide a 22G MR-compatible spinal needle (Somatex, Berlin, Germany) manually into the CM compartment. Needle placement was verified by drainage of CSF from the hub of the needle or by manual aspiration. Samples were collected at baseline CSF for each animal. Then, the needle was connected to an infusion system that consisted of extension tubing (Smiths Medical, Dublin, OH) and a 5-mL syringe filled with AAV vector. The 5-mL syringe was mounted onto an MR-compatible pump (Medfusion 3500, Medfusion, St. Paul, MN).

After acquiring a T1-weighted baseline scan to verify the location of the needle tip, vector dosing consisted of either an acute injection at a rate of 1 mL/min or a continuous injection at a rate of 1 mL/hr. Animals received a 6-mL volume through the CM route. T1-weighted MRI was acquired serially during the dosing procedure to monitor gadoteridol distribution in the CSF space. At 5 min after the dosing was completed, the infusion system was disconnected at the needle hub, intrathecal positioning of the needle tip was confirmed by visualizing CSF drainage, and the needle was removed. The animal was observed for full recovery from anesthesia and returned to its home cage.

Lumbar Injection

Three animals received a single lumbar injection, and two animals received a combined CM + lumbar injection. Briefly, the head, neck, and back were shaved and prepared for the vector injection into the CSF. The animal was placed on inhaled isoflurane (1%–3%) anesthesia, transferred to the MR suite, and was placed right on its right side in the MR scanner bed. A pelvic phased-array surface coil was positioned over the head and upper neck region. To facilitate lumbar access, the spine was slightly flexed by drawing the animal's hind limbs forward toward the umbilicus and widening the intervertebral space. Aseptic techniques were used to guide a 22G MR-compatible spinal needle (Somatex, Berlin, Germany) manually into the CM compartment and/or intrathecal lumbar space. Needle placement was verified by drainage of CSF from the hub of the needle or by manual aspiration. Samples were collected at baseline CSF for each animal. Then, the needle was connected to an infusion system that consisted of extension tubing (Smiths Medical, Dublin, OH) and a 5-mL syringe filled with AAV vector. The 5-mL syringe was mounted onto an MR-compatible pump (Medfusion 3500, Medfusion, St. Paul, MN).

After acquiring a T1-weighted baseline scan to verify the location of the needle tip, vector dosing consisted of either an acute injection at a rate of 1 mL/min or a continuous injection at a rate of 1 mL/hr. Animals received a 6-mL volume through the lumbar route. For the combined injection, volumes were divided in half and infused into the CM (3 mL) and lumbar (3 mL) space. T1-weighted MRI was acquired serially during the dosing procedure to monitor gadoteridol distribution in the CSF space. At 5 min after the dosing was completed, the infusion system was disconnected at the needle hub, intrathecal positioning of the needle tip was confirmed by visualizing CSF drainage, and the needle was removed. The animal was observed for full recovery from anesthesia and returned to its home cage.

Lateral Ventricle Injection

Two animals received bilateral infusions of vector with intraoperative MR guidance into the lateral ventricle (3 mL/hemisphere). Briefly, the animal was placed on inhaled isoflurane (1%–3%), and the head was shaved and positioned in an MR-compatible stereotactic frame. An aseptic bilateral craniectomy was performed in the prefrontal area to implant two MR-compatible cannula-guide devices onto the skull (one per hemisphere). After placement of the cannula guides, the wound site was temporarily closed, and the animal was transferred to the MR scanner. High-resolution MR scans were acquired to identify anatomical targets and to monitor infusate distribution. The infusion system consisted of a 16G adjustable stepped catheter (SmartFlow cannula, MRI Interventions, Irvine, CA, USA) connected via extension tubing to a 5-mL syringe mounted onto an MR-compatible infusion pump (Medfusion 3500, Medfusion, St. Paul, MN).

Each cannula was manually inserted through the guide-stem into the lateral ventricle, and positioning was verified by MRI. Vector dosing consisted of simultaneous infusions into the lateral ventricle of each hemisphere at a rate of 1 mL/min. T1-weighted MR was acquired serially during the dosing procedure to monitor gadoteridol distribution in the CSF surrounding the brain and spinal cord. After completion of the MR-guided infusions, the cannula was rested inside for 5 min to normalize intraventricular pressure and avoid backflow. The animal was returned to surgery where the cannula guides were removed and the incision closed in anatomical layers. The animal was transferred to its home cage and monitored for full recovery from anesthesia.

MR Image Acquisition and Analysis

T1-weighted images of the primate brain and spinal cord were acquired on a 1.5T Signa HDxt scanner (GE Medical Systems, Waukesha, WI). Intrathecal administration was monitored with either the head or the body coil. Prior to dosing, three-dimensional spoiled gradient echo (3D magnetization-prepared gradient echo) images were taken with a repetition time (TR)/echo time (TE)/flip angle = 4.0 ms/1.02 ms/15°, number of excitations (NEX) = 4, matrix = 256 × 512, field of view (FOV) = 4 × 12 cm, and slice thickness = 1.0 mm. Lateral ventricle administration images were acquired with a head coil. 3D spoiled gradient recalled (SPGR) images were acquired with a TR/TE/flip angle = 3.9 ms/1.54 ms/15°, NEX = 4, matrix = 256 × 192, FOV = 16 × 12 cm, and slice thickness = 1.0 mm. SPGR scans were acquired consecutively throughout the infusion procedure (acquisition time was ∼4 min per sequence) to monitor distribution from the cannula tip.

Infusion sites, cannula tracts, and cannula tip were identified on T1-weighted MR images in the coronal, axial, and sagittal planes with Osirix (Geneva, Switzerland). Regions of interest were delineated to outline T1 gadoteridol signal. Three-dimensional volumetric

reconstructions of the image series and regions of interest were analyzed with Brainlab iPlan Flow Suite (Brainlab, Munich, Germany) to estimate infusate distribution.

qPCR

qPCR was used for vector quantification as previously described.[39] Data are reported as the number of double-stranded hASM cDNA molecules per milliliter CSF. The qPCR primers and probe anneal to a 121-bp region of exons 2 and 3 of the ASM gene (nucleotides 219–339; HUGO Gene Nomenclature Committee [HGNC]: 11,120), thus spanning an intron that is not present in the vector sequence and thereby minimizing amplification of genomic DNA (forward primer, 5′-AGA CAC GTT TGA GGA CAT CA-3′; reverse primer, 5′-AAG CAT GGC CGG GTA CG-3′; TaqMan probe, 5′-6FAM-TGA CGC ACT GGC ACA GCC CCT ACT-TAMRA-3′; Applied Biosystems, Foster City, CA). The specificity of the primer and probe set was confirmed by running the reaction product on an agarose gel and detecting the amplicon of the predicted size. The qPCR analysis of AAV9-hASM-HA with a fluorogenic 5′-nuclease assay was performed on an Applied Biosystems 7900HT Sequence Detection System. Real-time qPCR was standardized with plasmid DNA containing the vector insert. The plasmid was linearized with a restriction enzyme, purified, quantified by ultraviolet absorbance, and diluted in qPCR dilution buffer to result in seven standards ranging from 1.0×10^1 to 1.0×10^6 copies/reaction.

Capsid Kinetics Assessment

CSF vector titer-time data from individual animals were analyzed by a non-compartmental analysis method. The following kinetic parameters were observed or calculated: C_{max}; T_{max}; apparent terminal rate constant (λ_z) derived from the slope of the log-linear regression of the log-linear terminal portion of the vector titer-time curve up to 24 hr after the end of infusion; $T_{1/2}$ calculated as $0.693/\lambda_z$; AUC_{24h} as calculated by the logarithmic down trapezoidal summation method; AUC_{inf} as calculated by AUC_{24h} plus titer at 24 hr after the end of infusion/λ_z; and AUC_{28d} as calculated by the logarithmic down trapezoidal summation method.

SUPPLEMENTAL INFORMATION

Supplemental Information includes Supplemental Materials and Methods, four figures, and three tables and can be found with this article online at https://doi.org/10.1016/j.omtm.2018.12.001.

AUTHOR CONTRIBUTIONS

K.O. and L.S. conducted experiments, generated and analyzed data, and wrote the paper. P.H. provided management and oversight. J.R.B., P.C.A., D.E.S., M.V.C., E.A.S., and G.G.C.H. carried out animal cage-side observation and welfare. V.S. processed tissue and generated data. C.S. processed tissue and managed laboratory resources. W.S.S. and J.N. reviewed and edited the paper. H.C. created the vector. J.F. provided oversight and reviewed and edited the paper. K.S.B. developed methodology, designed experiments, provided supervision and leadership, and reviewed the paper.

CONFLICTS OF INTEREST

P.C.A., D.E.S., M.V.C. and E.A.S. are paid employees of Valley Biosystems. H.C. is a paid employee of Virovek, Inc. The other authors declare no competing interests.

ACKNOWLEDGMENTS

We would like to thank Erik Pressley from DMS imaging Inc. for his assistance with MRI acquisition. Kinetics Foundation (USA) funded the present study.

REFERENCES

1. Su, X., Kells, A.P., Salegio, E.A., Richardson, R.M., Hadaczek, P., Beyer, J., Bringas, J., Pivirotto, P., Forsayeth, J., and Bankiewicz, K.S. (2010). Real-time MR imaging with Gadoteridol predicts distribution of transgenes after convection-enhanced delivery of AAV2 vectors. Mol. Ther. *18*, 1490–1495.
2. Salegio, E.A., Bringas, J., and Bankiewicz, K.S. (2016). MRI-Guided Delivery of Viral Vectors. Methods Mol. Biol. *1382*, 217–230.
3. Salegio, E.A., Samaranch, L., Kells, A.P., Forsayeth, J., and Bankiewicz, K. (2012). Guided delivery of adeno-associated viral vectors into the primate brain. Adv. Drug Deliv. Rev. *64*, 598–604.
4. Kells, A.P., Hadaczek, P., Yin, D., Bringas, J., Varenika, V., Forsayeth, J., and Bankiewicz, K.S. (2009). Efficient gene therapy-based method for the delivery of therapeutics to primate cortex. Proc. Natl. Acad. Sci. USA *106*, 2407–2411.
5. de Lange, E.C. (2013). Utility of CSF in translational neuroscience. J. Pharmacokinet. Pharmacodyn. *40*, 315–326.
6. Damkier, H.H., Brown, P.D., and Praetorius, J. (2013). Cerebrospinal fluid secretion by the choroid plexus. Physiol. Rev. *93*, 1847–1892.
7. Knopf, P.M., Cserr, H.F., Nolan, S.C., Wu, T.Y., and Harling-Berg, C.J. (1995). Physiology and immunology of lymphatic drainage of interstitial and cerebrospinal fluid from the brain. Neuropathol. Appl. Neurobiol. *21*, 175–180.
8. Duque, S.I., Arnold, W.D., Odermatt, P., Li, X., Porensky, P.N., Schmelzer, L., Meyer, K., Kolb, S.J., Schümperli, D., Kaspar, B.K., and Burghes, A.H. (2015). A large animal model of spinal muscular atrophy and correction of phenotype. Ann. Neurol. *77*, 399–414.
9. Federici, T., Taub, J.S., Baum, G.R., Gray, S.J., Grieger, J.C., Matthews, K.A., Handy, C.R., Passini, M.A., Samulski, R.J., and Boulis, N.M. (2012). Robust spinal motor neuron transduction following intrathecal delivery of AAV9 in pigs. Gene Ther. *19*, 852–859.
10. Samaranch, L., Salegio, E.A., San Sebastian, W., Kells, A.P., Bringas, J.R., Forsayeth, J., and Bankiewicz, K.S. (2013). Strong cortical and spinal cord transduction after AAV7 and AAV9 delivery into the cerebrospinal fluid of nonhuman primates. Hum. Gene Ther. *24*, 526–532.
11. Gray, S.J., Nagabhushan Kalburgi, S., McCown, T.J., and Jude Samulski, R. (2013). Global CNS gene delivery and evasion of anti-AAV-neutralizing antibodies by intrathecal AAV administration in non-human primates. Gene Ther. *20*, 450–459.
12. Samaranch, L., Sebastian, W.S., Kells, A.P., Salegio, E.A., Heller, G., Bringas, J.R., Pivirotto, P., DeArmond, S., Forsayeth, J., and Bankiewicz, K.S. (2014). AAV9-mediated expression of a non-self protein in nonhuman primate central nervous system triggers widespread neuroinflammation driven by antigen-presenting cell transduction. Mol. Ther. *22*, 329–337.
13. Samaranch, L., Salegio, E.A., San Sebastian, W., Kells, A.P., Foust, K.D., Bringas, J.R., Lamarre, C., Forsayeth, J., Kaspar, B.K., and Bankiewicz, K.S. (2012). Adeno-associated virus serotype 9 transduction in the central nervous system of nonhuman primates. Hum. Gene Ther. *23*, 382–389.
14. Meyer, K., Ferraiuolo, L., Schmelzer, L., Braun, L., McGovern, V., Likhite, S., Michels, O., Govoni, A., Fitzgerald, J., Morales, P., et al. (2015). Improving single injection CSF delivery of AAV9-mediated gene therapy for SMA: a dose-response study in mice and nonhuman primates. Mol. Ther. *23*, 477–487.
15. Hinderer, C., Bell, P., Katz, N., Vite, C.H., Louboutin, J.P., Bote, E., Yu, H., Zhu, Y., Casal, M.L., Bagel, J., et al. (2018). Evaluation of Intrathecal Routes of Administration for Adeno-Associated Viral Vectors in Large Animals. Hum. Gene Ther. *29*, 15–24.

16. Hinderer, C., Bell, P., Vite, C.H., Louboutin, J.P., Grant, R., Bote, E., Yu, H., Pukenas, B., Hurst, R., and Wilson, J.M. (2014). Widespread gene transfer in the central nervous system of cynomolgus macaques following delivery of AAV9 into the cisterna magna. Mol. Ther. Methods Clin. Dev. *1*, 14051.

17. Epstein, N.E. (2017). Neurological complications of lumbar and cervical dural punctures with a focus on epidural injections. Surg. Neurol. Int. *8*, 60.

18. Eskey, C.J., and Ogilvy, C.S. (2001). Fluoroscopy-guided lumbar puncture: decreased frequency of traumatic tap and implications for the assessment of CT-negative acute subarachnoid hemorrhage. AJNR Am. J. Neuroradiol. *22*, 571–576.

19. Pierce, D.B., Shivaram, G., Koo, K.S.H., Shaw, D.W.W., Meyer, K.F., and Monroe, E.J. (2018). Ultrasound-guided lumbar puncture in pediatric patients: technical success and safety. Pediatr. Radiol. *48*, 875–881.

20. Ho, M.L., Campeau, N.G., Ngo, T.D., Udayasankar, U.K., and Welker, K.M. (2017). Pediatric brain MRI part 1: basic techniques. Pediatr. Radiol. *47*, 534–543.

21. Haughton, V., and Mardal, K.A. (2014). Spinal fluid biomechanics and imaging: an update for neuroradiologists. AJNR Am. J. Neuroradiol. *35*, 1864–1869.

22. Koliatsos, V.E., Clatterbuck, R.E., Nauta, H.J., Knüsel, B., Burton, L.E., Hefti, F.F., Mobley, W.C., and Price, D.L. (1991). Human nerve growth factor prevents degeneration of basal forebrain cholinergic neurons in primates. Ann. Neurol. *30*, 831–840.

23. Higgins, P.B., Shade, R.E., Rodríguez-Sánchez, I.P., Garcia-Forey, M., Tejero, M.E., Voruganti, V.S., Cole, S.A., Comuzzie, A.G., and Folli, F. (2016). Central GIP signaling stimulates peripheral GIP release and promotes insulin and pancreatic polypeptide secretion in nonhuman primates. Am. J. Physiol. Endocrinol. Metab. *311*, E661–E670.

24. Ziegler, R.J., Salegio, E.A., Dodge, J.C., Bringas, J., Treleaven, C.M., Bercury, S.D., Tamsett, T.J., Shihabuddin, L., Hadaczek, P., Fiandaca, M., et al. (2011). Distribution of acid sphingomyelinase in rodent and non-human primate brain after intracerebroventricular infusion. Exp. Neurol. *231*, 261–271.

25. Paul, G., Zachrisson, O., Varrone, A., Almqvist, P., Jerling, M., Lind, G., Rehncrona, S., Linderoth, B., Bjartmarz, H., Shafer, L.L., et al. (2015). Safety and tolerability of intracerebroventricular PDGF-BB in Parkinson's disease patients. J. Clin. Invest. *125*, 1339–1346.

26. Cohen-Pfeffer, J.L., Gururangan, S., Lester, T., Lim, D.A., Shaywitz, A.J., Westphal, M., and Slavc, I. (2017). Intracerebroventricular Delivery as a Safe, Long-Term Route of Drug Administration. Pediatr. Neurol. *67*, 23–35.

27. Samaranch, L., Hadaczek, P., Kells, A.P., Bringas, J.R., Stockinger, D., San Sebastian, W., Macayan, M., Samineni, S., Pivirotto, P., Forsayeth, J., and Bankiewicz, K.S. (2016). Slow AAV2 clearance from the brain of nonhuman primates and anti-capsid immune response. Gene Ther. *23*, 393–398.

28. Salegio, E.A., Kells, A.P., Richardson, R.M., Hadaczek, P., Forsayeth, J., Bringas, J., Sardi, S.P., Passini, M.A., Shihabuddin, L.S., Cheng, S.H., et al. (2010). Magnetic resonance imaging-guided delivery of adeno-associated virus type 2 to the primate brain for the treatment of lysosomal storage disorders. Hum. Gene Ther. *21*, 1093–1103.

29. Nonnenmacher, M., and Weber, T. (2012). Intracellular transport of recombinant adeno-associated virus vectors. Gene Ther. *19*, 649–658.

30. Snyder, R.O., and Francis, J. (2005). Adeno-associated viral vectors for clinical gene transfer studies. Curr. Gene Ther. *5*, 311–321.

31. Bernaud, J., Rossi, A., Fis, A., Gardette, L., Aillot, L., Büning, H., Castelnovo, M., Salvetti, A., and Faivre-Moskalenko, C. (2018). Characterization of AAV vector particle stability at the single-capsid level. J. Biol. Phys. *44*, 181–194.

32. Nedergaard, M. (2013). Neuroscience. Garbage truck of the brain. Science *340*, 1529–1530.

33. Suzuki, Y., Nakamura, Y., Yamada, K., Igarashi, H., Kasuga, K., Yokoyama, Y., Ikeuchi, T., Nishizawa, M., Kwee, I.L., and Nakada, T. (2015). Reduced CSF Water Influx in Alzheimer's Disease Supporting the β-Amyloid Clearance Hypothesis. PLoS ONE *10*, e0123708.

34. Saraiva, J., Nobre, R.J., and Pereira de Almeida, L. (2016). Gene therapy for the CNS using AAVs: The impact of systemic delivery by AAV9. J. Control. Release *241*, 94–109.

35. Samaranch, L., Blits, B., San Sebastian, W., Hadaczek, P., Bringas, J., Sudhakar, V., Macayan, M., Pivirotto, P.J., Petry, H., and Bankiewicz, K.S. (2017). MR-guided parenchymal delivery of adeno-associated viral vector serotype 5 in non-human primate brain. Gene Ther. *24*, 253–261.

36. Naidoo, J., Stanek, L.M., Ohno, K., Trewman, S., Samaranch, L., Hadaczek, P., O'Riordan, C., Sullivan, J., San Sebastian, W., Bringas, J.R., et al. (2018). Extensive Transduction and Enhanced Spread of a Modified AAV2 Capsid in the Non-human Primate CNS. Mol. Ther. *26*, 2418–2430.

37. Daadi, M.M., Pivirotto, P., Bringas, J., Cunningham, J., Forsayeth, J., Eberling, J., and Bankiewicz, K.S. (2006). Distribution of AAV2-hAADC-transduced cells after 3 years in Parkinsonian monkeys. Neuroreport *17*, 201–204.

38. San Sebastian, W., Kells, A.P., Bringas, J., Samaranch, L., Hadaczek, P., Ciesielska, A., Macayan, M., Pivirotto, P.J., Forsayeth, J., Osborne, S., et al. (2014). SAFETY AND TOLERABILITY OF MRI-GUIDED INFUSION OF AAV2-hAADC INTO THE MID-BRAIN OF NON-HUMAN PRIMATE. Mol. Ther. Methods Clin. Dev. *3*, 14049.

39. Cunningham, J., Pivirotto, P., Bringas, J., Suzuki, B., Vijay, S., Sanftner, L., Kitamura, M., Chan, C., and Bankiewicz, K.S. (2008). Biodistribution of adeno-associated virus type-2 in nonhuman primates after convection-enhanced delivery to brain. Mol. Ther. *16*, 1267–1275.